Fast Single Pulse Resolved Laser Induced Breakdown Spectroscopy (spr-LIBS) for In-Line Monitoring of Complete Film Removal in Ni/NiCr Thin-Film Systems

Sönke Vogel[*1], Savran Saltuk[1], Kirsten Bobzin[2], Max P. Möbius[2], Benedikt Schmidt[2], Julia Janowitz[2], Benedikt Borschlegel[1], and Christian Hinke[1]

[1]*Chair for Laser Technology (LLT), RWTH Aachen University, Germany*
[2]*Chair and Institute of Surface Engineering (IOT), RWTH Aachen University, Germany*
[*]*Corresponding author's e-mail: soenke.vogel@llt.rwth-aachen.de*

An in-line monitoring system for ultra-short pulsed (USP) laser ablation was developed and assessed to two-dimensionally map the complete removal of a thin film. This method enables single pulse resolved monitoring based on Laser Induced Breakdown Spectroscopy (LIBS) for pulse repetition rates of up to 4 MHz. The transition from one 1.5 µm thin layer to another during laser ablation was detected. The mapping with Energy-dispersive X-ray Spectroscopy and our method are in very good agreement. Furthermore, an enhancement of the signal contrast was achieved with GHz bursts.
DOI: 10.2961/jlmn.2026.01.2007
Keywords: laser induced breakdown spectroscopy, femtosecond, ultra-short pulsed, mapping

1. Introduction

In this study, we present an in-line process monitoring method for ultrashort-pulse laser structuring of thin-film systems. A single laser pulse both ablates material and simultaneously detects chemical elements in the resulting plasma. While laser-induced breakdown spectroscopy (LIBS) based on plasma emission is well established, single-pulse measurements at MHz repetition rates are required and, to date, have not been reported. Our system enables spatial mapping of specific elemental content during laser structuring, enabling closed-loop process control.

We use thin-film ablation as a relevant case study. The stack comprises Nickel (Ni) and Nickel–Chromium (NiCr) layers with nonuniform thicknesses and similar ablation thresholds. We spatially map plasma emission to identify regions where the top Ni layer is not fully removed and then selectively reprocess only those regions. This cycle is repeated until the Ni layer is completely ablated.

In LIBS, a laser pulse generates a plasma that emits a continuum via bremsstrahlung and radiative recombination; this continuum depends on plasma temperature and density and decays as the plasma expands and cools. For ultrashort-pulse excitation, the continuum typically decays within ~30 ns and is cooler than in short-pulse, reheated plasmas [1–4]. As electrons relax to lower energy states, they emit photons at characteristic wavelengths; the corresponding energy levels are well known for each element [5,6]. A second, time-delayed pulse (tens of picoseconds to a few nanoseconds) can reheat the plasma and enhance line emission [7,8].

Surface mapping with LIBS has been demonstrated previously, but with a primarily quantitative focus and sampling rates up to 1 kHz using strongly focusing collection optics [9–14].

Our goal is to demonstrate concurrent material ablation and spatially resolved, single-pulse resolved LIBS at industrially relevant conditions—specifically, single-pulse resolution at >0.1 MHz and fluences near the ablation-efficiency optimum. Prior approaches are unsuitable for in-line, single-pulse monitoring due to their low sampling rates and nonoptimal fluences for surface structuring.

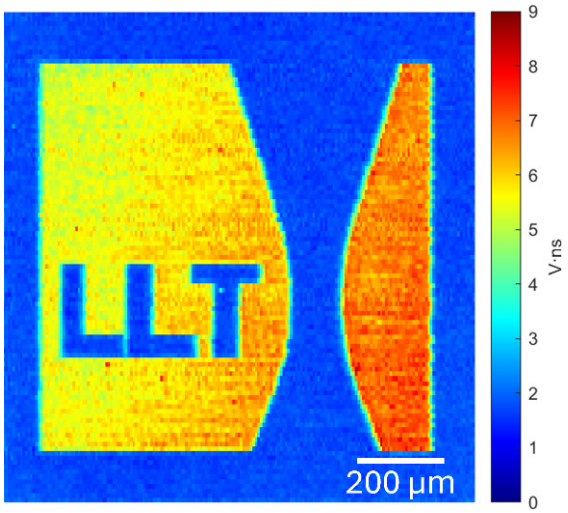

Fig. 1 Ablation of the Chair of Laser Technology's logo. The color encodes the 520.6 nm line emission intensity of Chromium. Higher line emissions indicate the presence of Chromium. The ablation was performed with 60 µJ pulse energy, 50 % pulse- and line-overlap and with 300 kHz repetition rate at a e^{-2} beam diameter of 14 µm. After every laser pulse the resulting line emission was recorded. Each pixel is one such measurement

2. Methods and Materials

First, we identified a sensor and emission line that enable single-pulse-resolved (spr) LIBS without integrating over multiple pulses. The emission line had to be strong and spectrally isolated to neighboring Nickel (Ni) or Chromium (Cr) lines and lie within a region of high detector responsivity. Conventional LIBS was performed to establish reference spectra and select a suitable emission line.

The conceived monitoring setup for spr-LIBS was then validated. The Cr to Ni and Cr to continuum emission ratio at the selected wavelength had to be high, independent of processing parameters, such as pulse energy, number of bursts, polarization or pulse duration. Furthermore, the system's sensitivity, even for line emission measurements of single pulses, was assessed.

Finally, we ablated two thin-film systems and, after each raster pass, produced spatial maps of the intensity of the selected Cr emission line on a per-pulse basis.

2.1 Material

Ni, Cr and Nickel-Chromium (Ni80Cr20, 80 wt.-% Ni, 20 wt.-% Cr) sputter targets (99.9 % purity, Kurt Lesker) were used for conventional LIBS and the signal intensity optimization experiments.

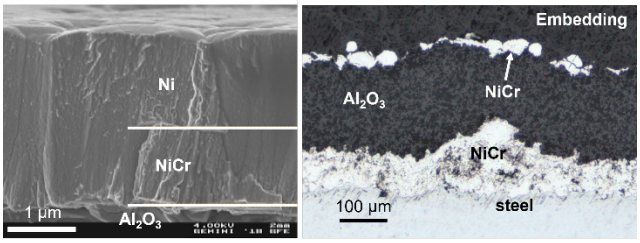

Fig. 2 Cross sections of film system 2 (left) and film system 1 (right).

Two thin film systems were utilized (Fig. **2**) for the spatial mapping experiments:

- Ni80Cr20 film (~20 µm thick) on an Aluminum-Oxide (Al_2O_3, 200 µm thick) insulation layer on another Ni80Cr20 film serving as adhesion layer between the steel substrate and the insulation layer.
- Ni (1.5 µm thick) on Ni80Cr20 (1.5 µm thick) on an Al_2O_3 insulation layer on a steel substrate.

The second film system was produced with physical vapor deposition and the first by thermal spraying. The ablation threshold of Ni and Ni80Cr20 is 0.11 J/cm^2.

Based on conventional LIBS results for Ni and Ni80Cr20, a monitoring setup was designed and coaxially integrated with the processing setup (Fig. 3). It consists of a backside-polished high reflection mirror for 1030 nm center wavelength, a high reflection mirror for 515 nm center wavelength and an optical bandpass filter (520 nm center wavelength, 20 nm FWHM). Since high repetition rates are necessary, a full spectrum cannot be recorded for every pulse. Therefore, a single amplified avalanche photodiode (APD13A2, Thorlabs) was employed to monitor the selected emission line of Cr at 520.6 nm. The signal was recorded with an oscilloscope (PD 5640, PicoScope). It was triggered by the laser's pulse picker.

The processing setup consists of a laser source (Pharos and Carbide, Light Conversion), a galvanometer scanner (excelliSCAN 20, ScanLab) and a F-Theta scanning optic (f=100 mm, Sill). The scanner mirrors are broadband coated (400 – 1100 nm). Their movement does not influence the recording of the line emission. At a scan-speed of 4000 m/s, the monitored position shifts by 1 µm, which is much smaller than the ablation diameter of ~30 µm.

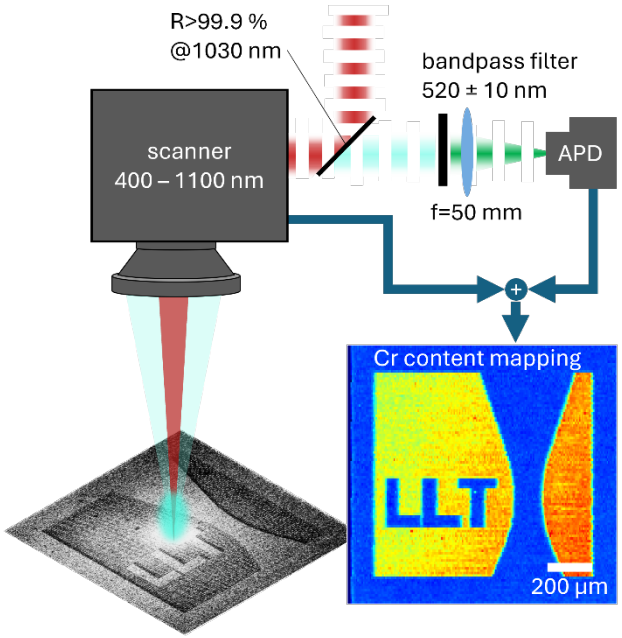

Fig. 3 Monitoring and processing setup.

2.2 Methods

The plasma emission spectra (conventional LIBS) of Ni and Ni80Cr20 during ultra-short pulsed laser ablation were recorded with an HR2000+ spectrometer (Ocean Optics). The ablation was performed at 1030 nm wavelength (Pharos, Light Conversion). The signal was integrated for 10 s. The laser was scanned across the sample with a 90 % pulse overlap with different pulse energies, ranging from 20 µJ to 200 µJ.

The spectrometer does not measure absolute intensities, which are required to select a sufficiently sensitive detector. Therefore, the following steps are performed to determine absolute intensities:

1. Measure the relative integrated intensity of the line emission and the continuum emission within the bandpass region of the filter between wavelengths λ_1 and λ_2.
2. Determine the plasma temperature T according to the Boltzmann distribution plot method [15,16].
3. Calculate the absolute radiance of a blackbody with the previously estimated temperature. The plasma surface area A is assumed to be a half sphere with a diameter equal to the ablation diameter D and an emissivity of 1. The incident radiance on the sensor is limited by the transmission of the individual components within the monitoring system and the solid angle of the scanning optics, subsumed in factor $L(\lambda)$, which depends on the wavelength λ:

$$S = \int_{\lambda_1}^{\lambda_2} L(\lambda) \cdot \frac{2\pi hc^2}{\lambda^5} \frac{1}{e^{hc/(\lambda k_B T)} - 1} A \, d\lambda. \quad (1)$$

4. Determine the absolute radiance of the spectral line from the absolute continuum emission radiance previously estimated and the ratio of the line emission and the continuum emission determined in step 1.

The following experiments were performed with a suitable sensor and the previously described processing and monitoring setup (Fig. 3). The 520.6 nm Cr emission line intensity was recorded with the monitoring setup at a sample rate of 5 GHz. The received signal was, as commonly performed in LIBS, integrated after a delay time of 48 ns, to filter out the plasma continuum emission (Fig. 7). For each data point the signals of 30 pulses were averaged.

We measured the influence of GHz bursts, as well as the pulse energy, the pulse duration and the polarization on the line emission intensity. The previously mentioned Ni80Cr20 and Ni sputter target were used for ablation and calibration of the monitoring setup.

For the spatial Cr distribution mapping, the Cr line emission intensity was measured as before. Furthermore, the current position of the laser beam on the sample was recorded in parallel to the line emission signal.

The Ni80Cr20 film in film system 1 was ablated with 60 µJ pulse energy and a pulse- and line-overlap of 50% and 25%, respectively. The e^{-2} beam diameter was 28 µm and the peak fluence was 19 J/cm^2. The spr-LIBS spatial Cr distribution was compared to a spatially resolved energy dispersive X-ray spectroscopy (EDX, QUANTAX EDS, Bruker nano GmbH) analysis of the Cr distribution. The resulting 2D spr-LIBS intensity map was binarized with a threshold of 30 % of the maximal signal and the edges were detected with a Canny filter.

The films system 2 was ablated with the same parameters except the beam diameter. It was decreased to 14 µm to increase the resolution. After every second layer the emission intensity was averaged over the ablated area and the ablation depth was measured with a laser scanning microscope (LSM, VK-9700, Keyence).

The monitoring setup was altered by introducing a polarizing beam-splitter and a λ/4 plate to circularly polarize the beam. It was noted that on polished samples the back-reflection triggers a second pulse from the laser source, incident on the sample with a delay of 8.5 ns. By passing the λ/4 plates two times, the laser beam's polarization is changed from p- to s-polarized and subsequently deflected by the polarizing beam-splitter. Thus, back-reflections into the source are prevented.

3. Results

Based on the recorded plasma emissions (Fig. 4), the 520.6 nm Cr emission line for the transition 3d5(6S)4p→ 3d5(6S)4s was selected for further discrimination between Ni80Cr20 and Ni. The plasma temperature was determined to be 5670 K (Fig. 10) with the peaks listed in Table 1. The ablation diameter was 32 µm. The solid angle of the lens was 0.005 and the transmissivity of the system was ca. 60 %. This resulted in an absolute average radiance of 1 µW for the continuum emission and 489 nW for the line emission. The sensor is required to output a minimal 5 mV signal for 1 % of the previously calculated value. Therefore, a sensor with a sensitivity of >10^5 V/W is required. The final monitoring setup was validated and neither the incident laser radiation nor other plasma emission lines were detected.

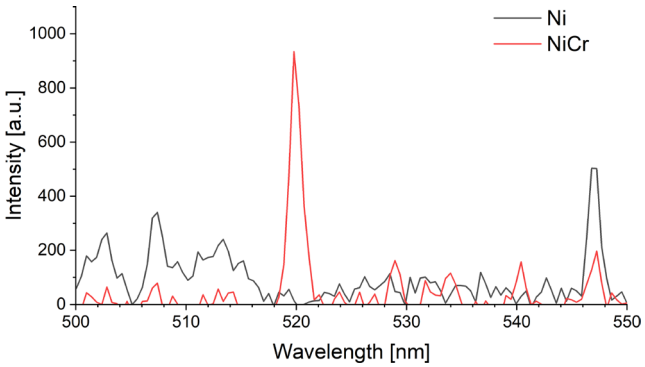

Fig. 4 Recorded LIBS spectrum with background emission removed.

The signal intensity for spr-LIBS at the 520.6 nm Cr emission line increased linearly with an increasing pulse energy. The slope was 0.06 V·ns/µJ. GHz bursts significantly increased the plasma emission intensity of Ni80Cr20 compared to Ni. For bursts with two sub-pulses the strongest intensity increase was observed. By increasing the number of pulses within the burst, no further increase was observed (Fig. 5). The inter-pulse temporal separation within the burst was 400 ps.

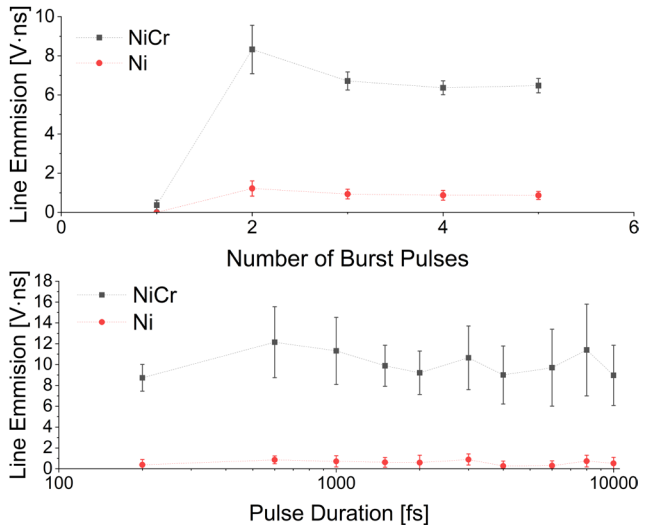

Fig. 5 Influence of the number of sub-pulses in a GHz burst on the emission signal (top). To avoid oversaturating the APD, the pulse energy was reduced to 30 µJ. For assessing the influence of the pulse duration (bottom) 120 µJ pulse energy was used.

As expected, the polarization angle did not change the emission intensity since the laser beam is incident perpendicular to the sample (Fig. 11). Circularly polarized laser radiation enhanced the continuum emission, but the line emission intensity did not change.

For film system 2 the low line-overlap of 25 % results in a rough ablated area (S_z=2.9 µm, S_q=0.59 µm). The measured Cr content increases with the ablated average depth and saturates at 3 µm average depth (Fig. 6d). For film system 1, a very good agreement between our method (spr-LIBS) and EDX was found (Fig. 6a+b).

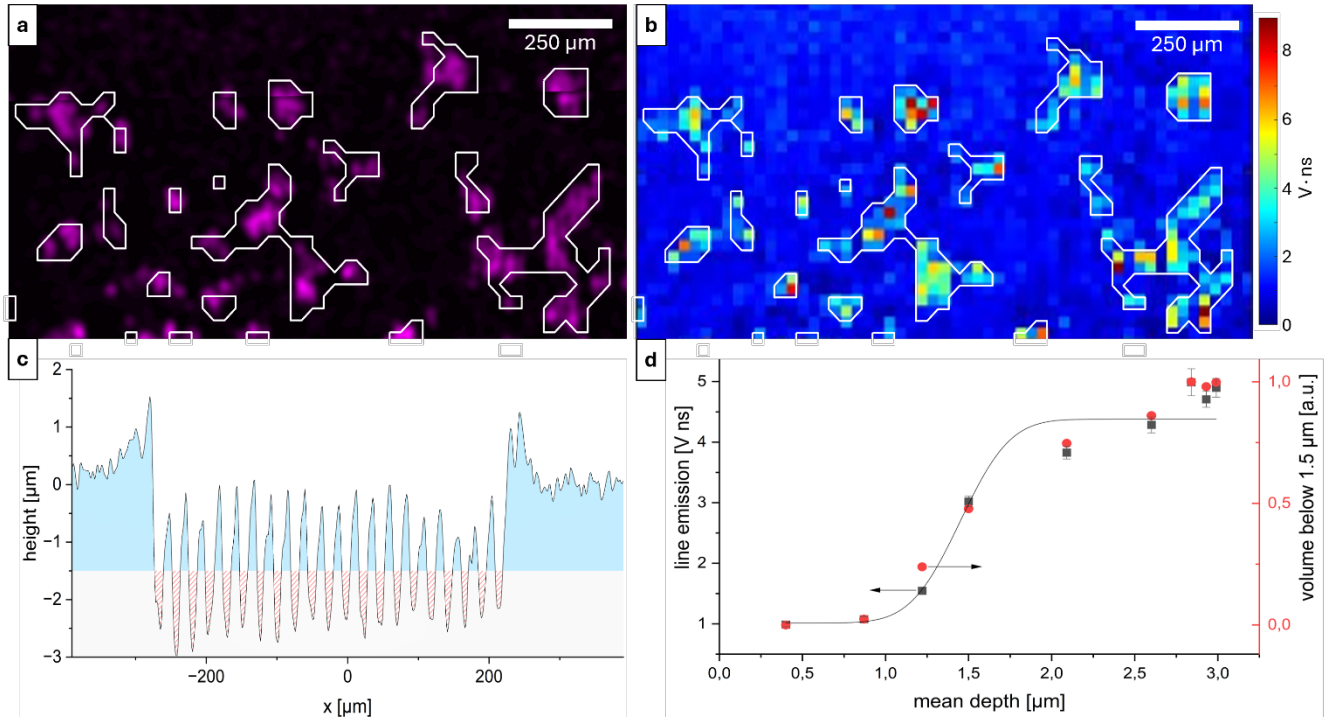

Fig. 6 EDX (**a**) and spr-LIBS (**b**) qualitative Cr mapping of the same laser ablated region for film system 1. The white lines are the detected edges of the binarized spr-LIBS signal. **c)** Cross section perpendicular to the scan direction after 12 scans for film system 2. The blue color encodes Ni80Cr20 and grey Ni. The red striped area highlights the volume below 1.5 µm. **d)** The average line emissions for the average depth at each layer (black) and the volume below 1.5 µm for each layer as depicted in **c)**. The black line is a fit to the line emission signal according to equation (5).

4. Discussion

The measured (~1 V) and theoretical LIBS plasma signals (0.6 V) are in good agreement. Other contributors to the signal other than the selected emission line are ruled out. The measured and the estimated photodiode voltage are in good agreement. However, the plasma temperature measured in this experiment might be estimated too high. A high pulse overlap was used for recording the spectra which might have increased the plasma temperature because of heat accumulation.

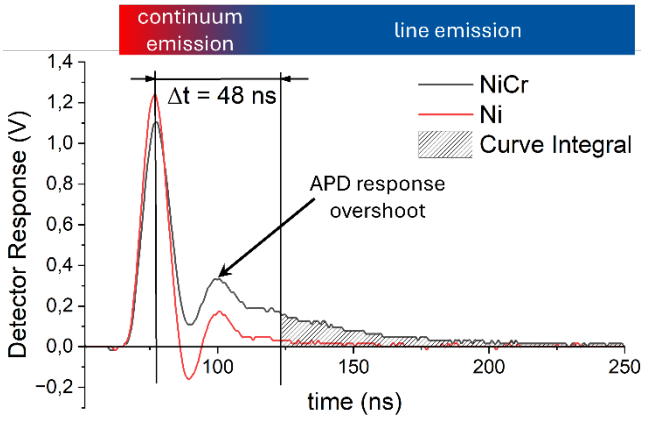

Fig. 7 Typical APD response on the plasma emission. The continuum emission is not taken into account by using a gate delay of 48 ns and a gate width of 200 ns.

Fig. 7 depicts the typical signal evolution recorded by the avalanche photodiode. First, a strong signal is observed which is attributed to the continuum emission. Then the plasma cools and the signal intensity decreases. For Ni, the signal even reaches negative values before a second peak is observed. This is attributed to the detecting RLC-circuit, consisting of a load resistor (R), a junction capacitance (C) and inductance (L). The observed signal is the typical transient response of an underdamped RLC circuit to a step input. The input in this case is the photodiode's response to the rapidly evolving continuum plasma. For NiCr, however, this typical response is overlapped by the line emission, which begins to evolve slower than the continuum emission but radiates longer. After around 50 ns the Ni's signal had vanished but the NiCr's signal was still present. This signal is associated with the line emission. Gating and integration of the detected signal is typically performed for LIBS. A gate delay of 48 ns and a gating window length of 200 ns has proven suitable for the present case.

The observed signal intensity enhancement for spr-LIBS generated with GHz bursts is in good agreement with other studies. An increasing pulse energy results in more, hotter plasma [4,17,18]. Bursts have been found previously to enhance the line emission intensity [2,8]. Subsequent pulses in a GHz burst reheat the already emerging plasma which in turn facilitates a stronger line emission [7,8].

Circularly polarized light was found to either enhance [19] or diminish the line intensity [20]. The plasma temperature increases for circular polarized excitation radiation [19]. In this work an increase in continuum emission was observed and a reduced line emission. The intensity of other emissions lines of either Ni or Cr might have been enhanced. However, the contribution of any emission line, except the 520.6 nm Cr emission line, was ruled out qua design and additionally the continuum emission was filtered out. Hence, only the 520.6 nm Cr emission line contributed to the signal.

Therefore, no signal enhancement for Ni was observed and any signal can be confidentially attributed to Cr.

The spr-LIBS resolution is low compared to the EDX analysis. EDX typically has a beam diameter of 1 µm, whereas the spr- LIBS ablation diameter is ca. 38 µm. Smaller patches of remaining Ni80Cr20 could not be detected. Moreover, the resolution is limited by the low pulse- and line overlap over 50 % and 25 %, respectively.

For film system 2 the transition from Ni to NiCr could be resolved. However, because of the low line-overlap a distinct sinusoidal pattern is observable perpendicular to the scan-direction (Fig. 6c). More Cr is detected at deeper parts. The average measured Cr content thereby resembles an average Cr content across multiple depths. For each layer, the volume, which is deeper than 1.5 µm (Figure 6) was measured. This resembles very accurately the measured Cr signal (Figure 7) and thereby confirms the former assumption.

The Cr content c_{Cr} in relation to the depth d is assumed to follow a distribution described by a Heaviside function H with the onset of the Ni80Cr20 layer at d_0:

$$c_{Cr} = c_{Cr,0}\, H(d - d_0). \tag{2}$$

The depth distribution D in one layer is described by a Gaussian distribution with the roughness value S_q.

$$D \sim A e^{-\frac{d}{S_q^2}}. \tag{3}$$

With the convolution theorem, one yields the expected average signal S for a given depth d:

$$S \sim \mathcal{F}^{-1}\{\mathcal{F}\{D\} * \mathcal{F}\{c_{Cr}\}\}. \tag{4}$$

By absorbing all constant and $c_{Cr,0}$ into A and accounting for a signal offset C, the signal is obtained by

$$S = C + A e r f\left(\frac{d - d_0}{S_q}\right). \tag{5}$$

The fit predicts the onset of the Ni80Cr20 film at d_0 = 1.44 µm and S_q = 0.33 µm. At deeper average depths, the deepest parts have already reached the isolating Al_2O_3 film and thus do not contribute to the Cr line emission. The assumption for the depth distribution becomes invalid and the model differs from the measured signal.

The Chair of Laser Technology's logo (Fig. 1) was scanned with 50 % line overlap, resulting in a smoother surface. It was scanned from left to right. Therefore, heat has accumulated at the right side, resulting in a deeper ablation, which in turn is mirrored by the Cr line emission. More Cr is detected on the right side as compared to the left side.

spr-LIBS is applicable for in-line monitoring of qualitative element detection. The state of the art in terms of sampling frequency has been exceeded by a factor of 200, even though the laser source was eventually limiting higher pulse repetition rates. The signal was integrated up to 250 ns after the laser pulse. Therefore, a theoretical pulse repetition rate of 4 MHz should be possible. However, interaction of the ejection plume of a previous pulse might influence the signal at such high repetition rates. Moreover, the redeposition of ejected particles could influence the signal. On the other hand, this might be seen as a chance to clean such deposits with an additional pass.

The proposed system also lacks adaptability. A further upgrade could be the inclusion of a grating with multiple APDs. Still, the versatility of a CCD sensor is unmatched. Additionally, non-overlapping emission lines must be present. The storage capability of the oscilloscope limits the processable areas. Almost 1 Gb of data is saved for a 2 mm x 2 mm area for 200 kHz repetition rate and a scan speed of 2000 m/s. With an electronic circuit, which gates and integrates the signal, the required data could be reduced by a factor of 50 000. If the plasma emission remains in focus even at the scan field edges was not tested.

Even though, the spatial resolution increases with decreasing beam diameter, a reduction to previously used beam diameters [9,12,14] is not commercially viable.

5. Conclusion

We have proven that ultra-fast in-line detection based on LIBS is possible. Laser ablation results in specific line emission, which was detected for every individual pulse at a repetition rate of 200 kHz. The qualitative spatially resolved Cr content measurement with our method – single pulse resolved LIBS – was in very good agreement with EDX determined Cr distribution. Moreover, our method was expanded to 3D detection. The transition from a Ni to a Ni80Cr20 thin film was measured during laser ablation.

Acknowledgements

Funded by the Deutsche Forschungsgemeinschaft (DFG, German Research Foundation) under Germany's Excellence Strategy – EXC-2023 Internet of Production – 390621612.

Appendix A

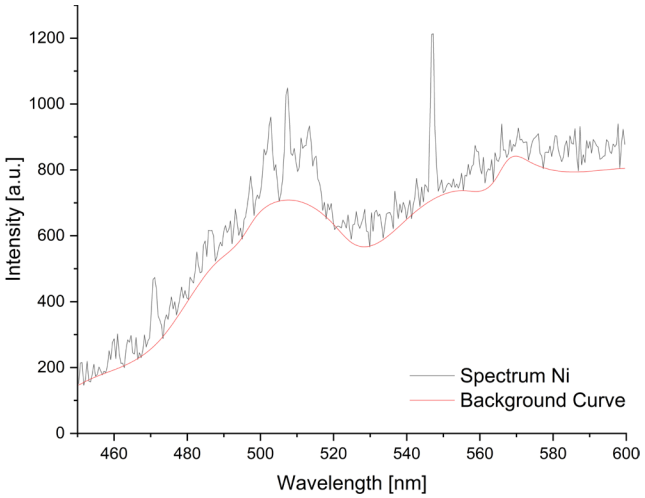

Fig. 8 Acquired raw Ni spectrum and calculated background curve.

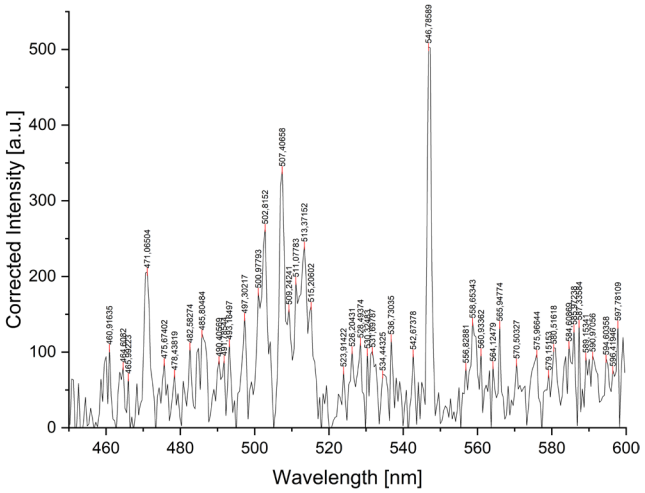

Fig. 9 Ni spectrum with removed background and detected peaks used for the Boltzmann plot method.

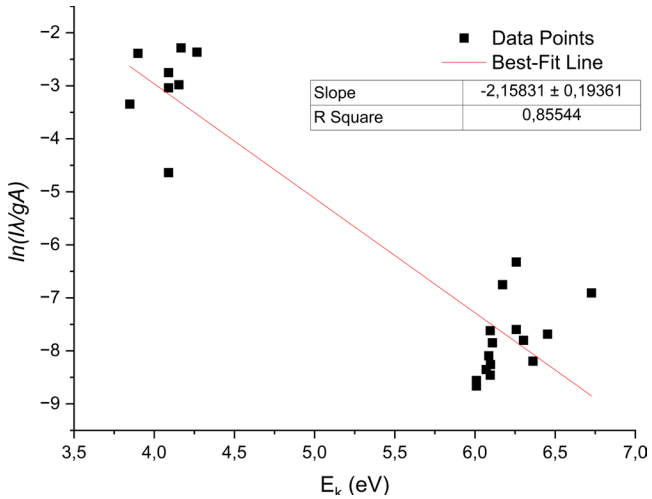

Fig. 10 Boltzmann plot for Ni.

Table 1 Necessary data for the Boltzmann plot [16]

Center Wave-length [nm]	Peak Inten-sity [a.u.]	Listed Wave-length [nm]	A $[s^{-1}]$	E_k $[eV]$	J_k	g_k
471.1	206.1	471.442	4.60E+07	6.0091	5	11
475.7	86.7	475.652	1.50E+07	6.0859	4	9
478.4	71.6	478.654	1.80E+07	6.0091	5	11
482.6	107.6	482.903	1.90E+07	6.1089	3	7
485.8	124.5	485.541	5.70E+07	6.0949	2	5
490.4	89.5	490.441	6.20E+07	6.0694	1	3
491.8	90.5	491.836	2.30E+07	6.3611	3	7
493.2	111.9	493.583	2.40E+07	6.4522	2	5
501	179.7	501.246	1.10E+07	6.1716	3	7
502.8	264.3	503.537	5.70E+07	6.0969	4	9
507.4	340.4	508.052	3.20E+07	6.0949	5	11
511.1	194.3	511.54	2.20E+07	6.2570	4	9
513.4	240.9	513.708	8.60E+05	4.0893	1	3
515.2	161.1	515.576	2.90E+07	6.3024	3	7
542.7	98.4	543.587	1.90E+05	4.2661	1	3
546.8	503.3	547.691	9.50E+06	4.0893	1	3
556.8	80.6	557.873	9.80E+04	3.8983	2	5
558.7	140	558.786	2.20E+05	4.1536	3	7
560.9	100	559.228	1.10E+05	4.1672	2	5
565.9	136	566.402	1.10E+07	6.7263	3	7
570.5	86.5	570.956	2.00E+05	3.8474	3	7
576	98	576.085	3.50E+06	6.2570	4	9
589.2	94.2	589.288	2.90E+05	4.0893	1	3

Appendix B

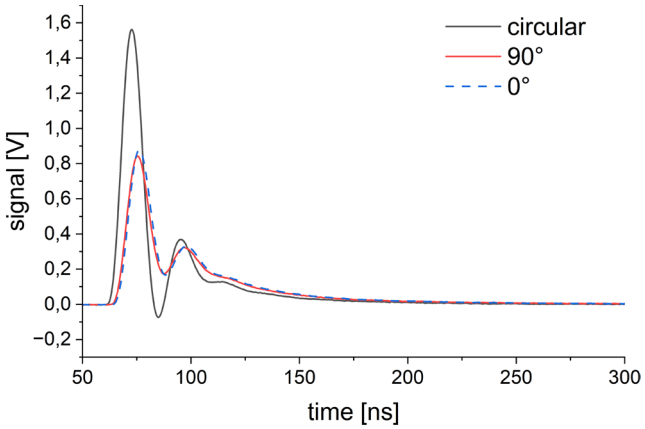

Fig. 11 Measured plasma signal for excitation with linear and circular polarized laser radiation. The linear polarization direction was rotated by 90°.

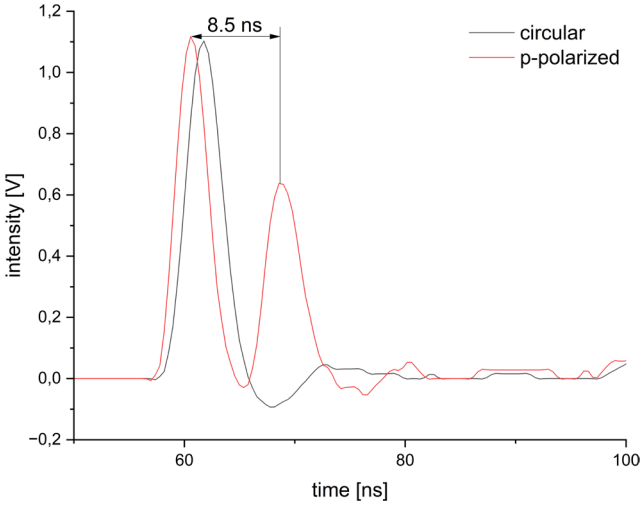

Fig. 12 Generation of a second pulse in the source, reflected from a polished Ni sample for p-polarized laser radiation and amplified in the laser source. With a λ/4 plate and a beam splitter the back-reflection is suppressed (circular).

References

[1] B. Le Drogoff, J. Margot, M. Chaker, M. Sabsabi, O. Barthélemy, T. W. Johnston, S. Laville, F. Vidal, and Y. von Kaenel: Spectrochim. Acta B: At. Spectrosc., 56, (2001) 987.

[2] A. Semerok and C. Dutouquet: Thin Solid Films, 453-454, (2004) 501.

[3] F. Anabitarte, A. Cobo, and J. M. Lopez-Higuera: ISRN Spectrosc., (2012) 285240.

[4] C. M. Ahamer, K. M. Riepl, N. Huber, and J. D. Pedarnig: Spectrochim. Acta B: At. Spectrosc. 136, (2017) 56.

[5] J. P. Singh: Laser-Induced Breakdown Spectroscopy, 2nd ed. (Elsevier Science & Technology, San Diego, 2020), 20.

[6] R. Noll: Laser-Induced Breakdown Spectroscopy. Fundamentals and Applications, (Springer Berlin / Heidelberg, Berlin, Heidelberg, 2012), 8.

[7] S. S. Harilal, P. K. Diwakar, and A. Hassanein: Appl. Phys. Lett., 103, (2013) 041102.

[8] C. M. Ahamer and J. D. Pedarnig: Spectrochim. Acta B: At. Spectrosc., 148, (2018) 23.

[9] Z. Wang, S. Shen, Y. Arima, C. Li, W. Zhou, S. Li, J. Yan, and Y. Deguchi: Spectrochim. Acta B: At. Spectrosc., 220, (2024) 107016.

[10] D. Menut, P. Fichet, J.-L. Lacour, A. Rivoallan, and P. Mauchien: App. Opt., 42, (2003) 6063.

[11] L. Jolivet, M. Leprince, S. Moncayo, L. Sorbier, C.-P. Lienemann, and V. Motto-Ros: Spectrochim. Acta B: At. Spectrosc., 151, (2019) 41.

[12] H. Bette and R. Noll, J. Phys. D: Appl. Phys., 37, (2004) 1281.

[13] R. Noll, H. Bette, A. Brysch, M. Kraushaar, I. Mönch, L. Peter, and V. Sturm: Spectrochim. Acta B: At. Spectrosc., 56, (2001) 637.

[14] S.-J. J. Tsai, S.-Y. Chen, Y.-S. Chung, and P.-C. Tseng: Anal. Chem., 78, (2006) 7432.

[15] B. Bousquet, V. Gardette, V. M. Ros, R. Gaudiuso, M. Dell'Aglio, and A. de Giacomo: Spectrochim. Acta B: At. Spectrosc., 204, (2023) 106686.

[16] A. Kramida and Y. Ralchenko: NIST Atomic Spectra Database, NIST Standard Reference Database, 78, (1999).

[17] K. L. Eland, D. N. Stratis, D. M. Gold, S. R. Goode, and S. M. Angel: Appl Spectrosc 55, (2001) 286.

[18] Q. Wang, A. Chen, H. Qi, S. Li, Y. Jiang, and M. Jin: Opt. Laser Technol., 121, (2020) 105773.

[19] Q. Wang, A. Chen, W. Xu, S. Li, Y. Jiang, and M. Jin: J. Anal. At. Spectrom., 34, (2019) 1242.

[20] U. K. Adarsh, V. K. Unnikrishnan, P. Vasa, S. D. George, S. Chidangil, and D. Mathur: Appl. Phys. B, 129, (2023) 185.

(Received: July 1, 2025, Accepted: December 21, 2025)